Morphological Stabilization by In Situ Polymerization of Fullerene Derivatives Leading to Efficient, Thermally Stable Organic Photovoltaics

Yen-Ju Cheng, Chao-Hsiang Hsieh, Pei-Jung Li, and Chain-Shu Hsu**

The successful design and synthesis of two styryl-functionalized fullerene derivatives, [6,6]-phenyl-C_{61}-butyric acid styryl dendron ester (PCBSD) and [6,6]-phenyl-C_{61}-butyric acid styryl ester (PCBS) is presented. The polymerizable PCBS or PCBSD materials are incorporated into a poly(3-hexylthiophene) (P3HT):[6,6]-phenyl-C61-butyric acid methyl ester (PCBM) blend to form an active layer of ternary blend. The blending systems are first thermally annealed at 110 C for 10 min to induce optimal morphology, followed by heating at 150 C for 10 min to trigger the in situ polymerization of styrene groups. Through chemical crosslinking of PCBSD, the initial morphology of the blend (P3HT:PCBM:PCBSD = 6:5:1 in weight) can be effectively fixed and stably preserved. The device based on this blend shows extremely stable device characteristics, delivering an average power conversion efficiency (PCE) of 3.7% during long-term thermal treatment. By molecular engineering to reduce the insulating portion, PCBS with higher C_{60} content (71 wt%) possesses better electron-transport properties than PCBSD (58 wt%). Encouragingly, at a low doping concentration of PCBS in the blend (P3HT:PCBM:PCBS = 6:5:1 in weight), linear-polymerized PCBS can stabilize the morphology against thermal heating. This device exhibits more balanced charge mobility to achieve an average PCE of 3.8% over 25 h heating at 150 °C.

1. Introduction

Polymer solar cells (PSCs) are a promising alternative for clean and renewable energy due to their potential to be fabricated onto large area, light-weight flexible substrates by solution processing at lower cost. The general working principle in such solar cells first involves photoexcitation of the donor material by absorption of light energy to generate excitons. This Coulomb-correlated electron–hole pair diffuses to the donor–acceptor (D–A) interface, where exciton dissociation occurs. Because their limited lifetimes only allow excitons to diffuse a short distance (5–14 nm),[1] donor excitons created far away from the heterojunction interface decay to the ground state before they reach the D–A interfaces, which leads to the loss of absorbed photons and quantum efficiency. PSCs based on the concept of bulk heterojunction (BHJ) strategy have provided the most straightforward solutions to maximize internal D–A interfacial area for efficient charge separation thus far, but tailoring the morphology of the blend in a BHJ device toward optimized performance is of critical importance and remains challenging. Until now, the combination of poly(3-hexylthiophene) (P3HT) as electron donor and [6,6]-phenyl-C_{61}-butyric acid methyl ester (PCBM) as electron acceptor in the active layer represents one of the most efficient BHJ solar cells, with power-conversion efficiencies approaching 5%.[2] The success of the P3HT:PCBM system mostly relies on carefully controlling the phase separation between two components in the bulk to reach an ideal morphology with D–A domain size around 10 nm, which is comparable to the diffusion length of excitons. The morphological development of the P3HT:PCBM blend is governed not only by intrinsic molecular properties but also by the extrinsic processing conditions of devices. For example, the regioregularity,[3] molecular weight,[4] and polydispersity[5] of P3HT are important structural factors that greatly influence its crystallinity; thus, variation of these factors can result in different morphologies of polymer blends. More importantly, the kinetics of crystallization and segregation of the P3HT:PCBM components can be manipulated by many parameters, including casting solvent, blending ratio,[6] external treatment of solvent annealing, and thermal annealing.[7] Thermal annealing of P3HT:PCBM composite provides external energy, which drives the P3HT to reorganize and self assemble to become crystalline P3HT. Through this morphological evolution, the featureless and homogeneous blend gradually reaches a bicontinuous interpenetrating D–A network with optimal D–A domain size.[2a] As a result, maximum interfacial area for efficient charge generation and a higher degree of nanoscale P3HT crystallinity can be achieved for better charge transport.[8] Unfortunately, this optimal morphology is a kinetically trapped intermediate that readily moves toward a more thermodynamically stable state if thermal annealing at elevated temperature is applied constantly.[9] The P3HT domain continues to undergo further crystallization, while the spherical PCBM, with its high

Prof. Y.-J. Cheng, C.-H. Hsieh, P.-J. Li, Prof. C.-S. Hsu
Department of Applied Chemistry
National Chiao Tung University
1001 Ta Hsueh Road Hsin-Chu, 30010, Taiwan
E-mail: yjcheng@mail.nctu.edu.tw; cshsu@mail.nctu.edu.tw

DOI: 10.1002/adfm.201002502

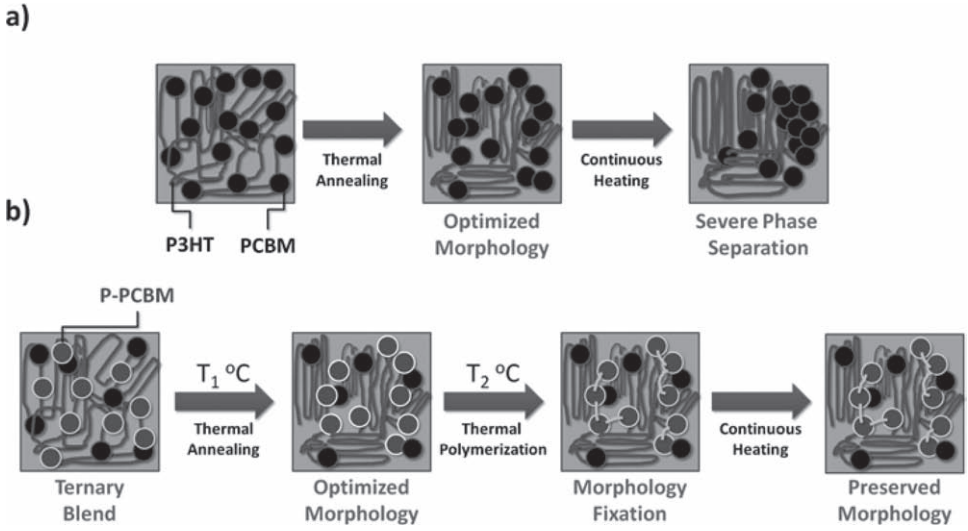

Figure 1. a) Morphological evolution of the P3HT:PCBM blend under thermal treatment. b) Two-stage thermal-annealing strategy of the P3HT:PCBM:P-PCBM blend to chemically lock the morphology and preserve the morphological stability ($T_1 < T_2$).

molecular mobility, tends to diffuse out of the polymer matrix and aggregate into larger clusters or single crystals.[9d,9e,10] Such a progressive phase segregation between P3HT and PCBM eventually leads to micronsized D–A domains with concomitant reduction of the D–A interfacial area, as shown in **Figure 1**a. Considering that a photovoltaic device must be exposed to long-term sunlight irradiation, the accumulated heat may raise the operational temperature above the glass transition temperature (T_g) of polymers, thus destroying the optimal morphology, and deteriorating the device performance.[11] Consequently, morphological instability of PSCs is considered to be one of the major obstacles that hinder its path toward commercialization. The development of new strategies to preserve optimal morphology is urgently needed but rather challenging. Fréchet and co-workers found that a slight decrease of the regioregularity of P3HT to weaken the crystallization-driven phase separation not only retains the device efficiency but also enhances the thermal stability of morphology in the solar cells.[12] Utilization of secondary interactions between donors and acceptors to fix morphology has also been explored.[13] Fréchet et al. used a diblock copolymer containing fullerene and oligothiophene pendant groups to serve as a compatibilizer to improve adhesion between the P3HT and PCBM boundaries.[13a] A more straightforward method is to lock morphology by covalent bonding.[14] In situ chemical crosslinking in BHJ films right after the formation of the optimal morphology is an ideal strategy to develop the desired morphology while improving morphological stability.[14] For this purpose, functionalities for crosslinking reactions should be incorporated into either p-type polymers[14a] or n-type fullerene derivatives.[14d,e] In the former case, photocrosslinkable P3HT copolymers used to blend with PCBM were developed to stabilize the BHJ film morphology.[14a] Because the polymeric 3D networks limit the conformational dynamics of the polymers and indirectly obstruct the diffusion pathway of PCBM molecules, efficient and stable photovoltaics could be realized. One potential drawback for this design is that the attachment of crosslinkers on the side chain of P3HT may disturb the π–π stacking of P3HT and alter the charge-transport properties.[15] Morphological studies have shown that PCBM molecules are capable of diffusing rapidly into crystalline P3HT upon thermal treatment; this ability is even more pronounced in an amorphous polymer matrix such as MDMO–PPV.[9c,d] We envisaged that direct crosslinking between highly mobile PCBM molecules to prevent them from severe immigration could be a more effective way to maintain optimal morphology. Moreover, compared to the numerous p-type conjugated polymers with excellent properties rapidly being developed, n-type materials are still exclusively dominated by PCBM-based derivatives. It would be more economical and practical, from the standpoint of synthetic feasibility, to develop a single polymerizable PCBM-based material that is widely applicable to all kinds of p-type polymers, regardless of whether they are amorphous or crystalline, to avoid large-scale phase separation. A PCBM derivative functionalized with an epoxy group as a polymerization group has been demonstrated.[14d] However, this system requires the addition of a catalytic amount of ionic photoinitiator, which turns out to be detrimental to the device due to the electron-trapping effect.

Styrene is known to be a superb thermally curable group because it undergoes efficient and rapid polymerization in the solid state to form polystyrene without the use of any initiators.[16] Herein, we have designed and synthesized two styryl-functionalized fullerene derivatives, [6,6]-phenyl-C_{61}-butyric acid styryl dendron ester (PCBSD)[17] and [6,6]-phenyl-C_{61}-butyric acid styryl ester (PCBS), to fine-tune the crosslinking and electron-transport properties (**Scheme 1**). The C_{60} weight contents in PCBSD and PCBS are 58% and 71%, respectively. PCBSD, containing a small dendron to attach two styrene groups, is more able than PCBS to efficiently lock morphology when blending with a p-type material, because the two styrene groups in PCBSD allow a 3D crosslinking reaction, whereas one styrene group in PCBS only allows linear polymerization. However, the high content of the insulating dendron in PCBSD may inevitably deteriorate its electron-transport properties and thereby decrease device performance. Therefore, PCBS should have better electron-transport properties than

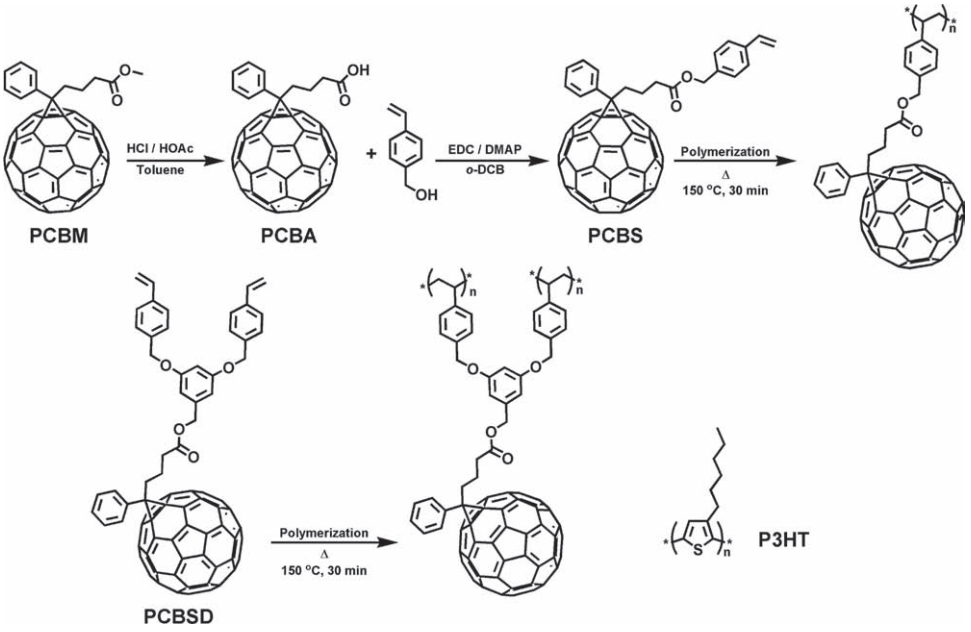

Scheme 1. The synthetic route for PCBS, the structure of PCBSD, and their thermal polymerization.

PCBSD. The core structure of PCBSD and PCBS is based on the most widely used n-type material, PCBM, so they are expected to inherit all the excellent electrical properties of PCBM. In addition to tailoring the materials' properties at molecular level, we can further adjust the macroscopic properties by varying the composition in the active layer. The polymerizable PCBM-based materials (P-PCBM), PCBS, or PCBSD, can be doped into the P3HT:PCBM system to form a ternary blend system P3HT/PCBM/P-PCBM. The relative content of P-PCBM to PCBM can be fine tuned for the purpose of morphological fixation without affecting the electron-transport properties in the active layer.

The temperature window required to drive the styrene groups to polymerize in these materials is just above the annealing temperature used to optimize the morphology of the P3HT:PCBM system, which allows us to accomplish the morphological fixation through a distinct two-stage process, as depicted in Figure 1b. Without the interference of chemical reactions, the optimized morphology under thermal annealing at T_1 °C is developed at the first stage, followed by sequentially triggering the chemical crosslinking at T_2 °C to preserve the morphology at the second stage, thereby leading to high-performance solar cells with excellent morphological stability.

2. Results and Discussion

2.1. Synthesis and Thermal Properties of the Styryl-Functionalized PCBM Derivatives

The synthesis of PCBSD has been previously reported.[17] PCBS was prepared by the esterification of PCBA with 4-vinylbenzyl alcohol in the presence of 1-ethyl-3-(3-dimethylaminopropyl) carbodiimide (EDC) and 4-dimethylaminopyridine (DMAP) in 69% yield.

The thermal-transition properties of PCBS and PCBSD monomers were investigated by the first scan of differential scanning calorimetry (DSC). It showed a broad exothermic peak with a T_{max} of around 150 °C, which clearly indicates thermal polymerization of styrene groups. In addition, the vibrational stretching of the vinyl groups at 1622 cm^{-1} in PCBS and PCBSD completely disappears in the IR spectrum after thermal treatment, which provides further evidence for polymerization. After the initial heating cycle, a high T_g of ca. 142 °C was observed during the second DSC scan, which indicates that the polymerized materials are highly amorphous. Thus, the polymerized materials can reduce the tendency toward crystallization and maintain long-term morphological stability.

2.2. Performances and Thermal Stability of BHJ Solar Cells

In this study, we use the conventional device configuration ITO/PEDOT:PSS/active layer/Ca/Al, and implement two-stage thermal annealing as the standard procedure for all of the blending systems. The spin-coated active-layer blend is first thermally annealed at 110 °C for 10 min to develop suitable morphology, followed by thermal annealing at 150 °C for another 10 min to trigger in situ polymerization. For comparison, we first fabricated a P3HT:PCBM-based (1:1 in wt%) reference device which exhibited a PCE value of 4.08% under AM 1.5G illumination (**Figure 2**a, and Table S1 in the Supporting Information). We then fabricated a device using P3HT:PCBSD as the active layer where the PCBM is completely replaced by the crosslinkable PCBSD. In this case, the weight ratio of the P3HT:PCBM:PCBSD blend is 1:0:1. For simplicity, we denote this blend as PCBSD101. Under AM 1.5G illumination at 100 mW/cm^2, device PCBSD101 showed very poor device performance with a power conversion efficiency (PCE) of 0.04% (Figure 2a). An obvious kink effect in the *J–V* curve was observed, which implies that a high degree of crosslinking and a high

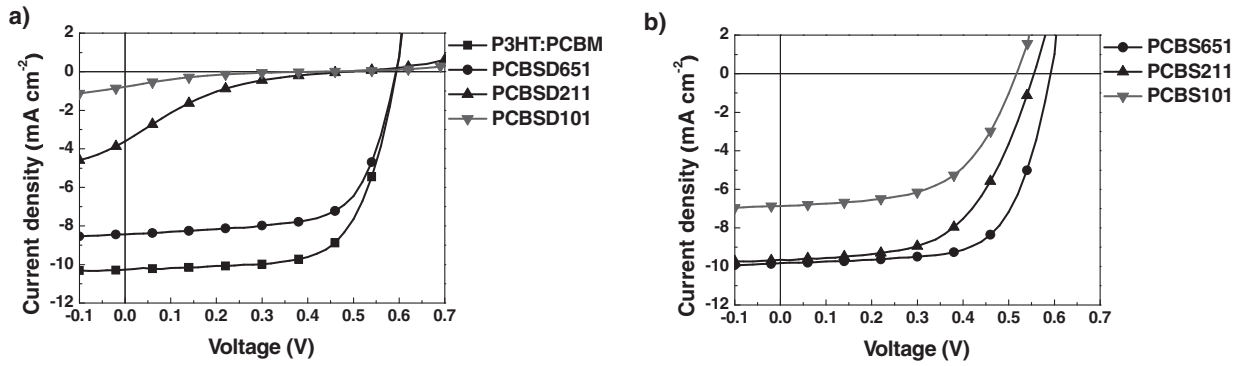

Figure 2. *J–V* characteristics of PSCs based on a) the P3HT:PCBM, PCBSD651, PCBSD211, and PCBSD101 blends, and b) PCBS651, PCBS211, and PCBS101 blends under AM 1.5 irradiation at 100 mW cm^{-2}.

content of insulating polystyrene in the n-type material domain exert a detrimental effect on the electron transport.

To improve the electron-transporter content in the composite, we incorporated PCBM into the P3HT:PCBSD blend to dilute the PCBSD content and form a ternary system. We fixed the blending weight ratio of P3HT to the total n-type materials (i.e., PCBM plus PCBSD) at 1:1 and adjusted the relative content between the PCBM and PCBSD. Devices PCBSD211 and PCBSD651 were fabricated using the P3HT:PCBM:PCBSD (2:1:1 in wt%) blend and the P3HT:PCBM:PCBSD (6:5:1 in wt%) blend, respectively. The PCE of device PCBSD211 was 0.23% better than that of device PCBSD101 (Figure 2a). By further decreasing the PCBSD content in the blend, the PCE of device PCBSD651 was dramatically improved to a reasonable value of 3.32% (Figure 2a).

To systematically evaluate the ability of PCBSD to stabilize morphology and preserve device characteristics under the influence of thermal treatment, we fabricated a series of devices identical in all aspects except that the P3HT:PCBM:PCBSD (6:5:1 in wt%) thin films, prepared by the standard procedure, were further isothermally heated to 150 °C for various times prior to deposition of the top electrode. The corresponding reference devices based on the P3HT:PCBM system were also fabricated and characterized to test thermal stability. The *J–V* curves of the P3HT:PCBM reference and PCBSD651 devices are shown in **Figure 3**a and b, respectively, and their corresponding photovoltaic parameters (PCE, V_{oc}, J_{sc} and fill factor (FF)) as functions of heating time at 150 °C were plotted in **Figure 4**. It can be seen that the performance of the P3HT:PCBM reference device decreases as the heating

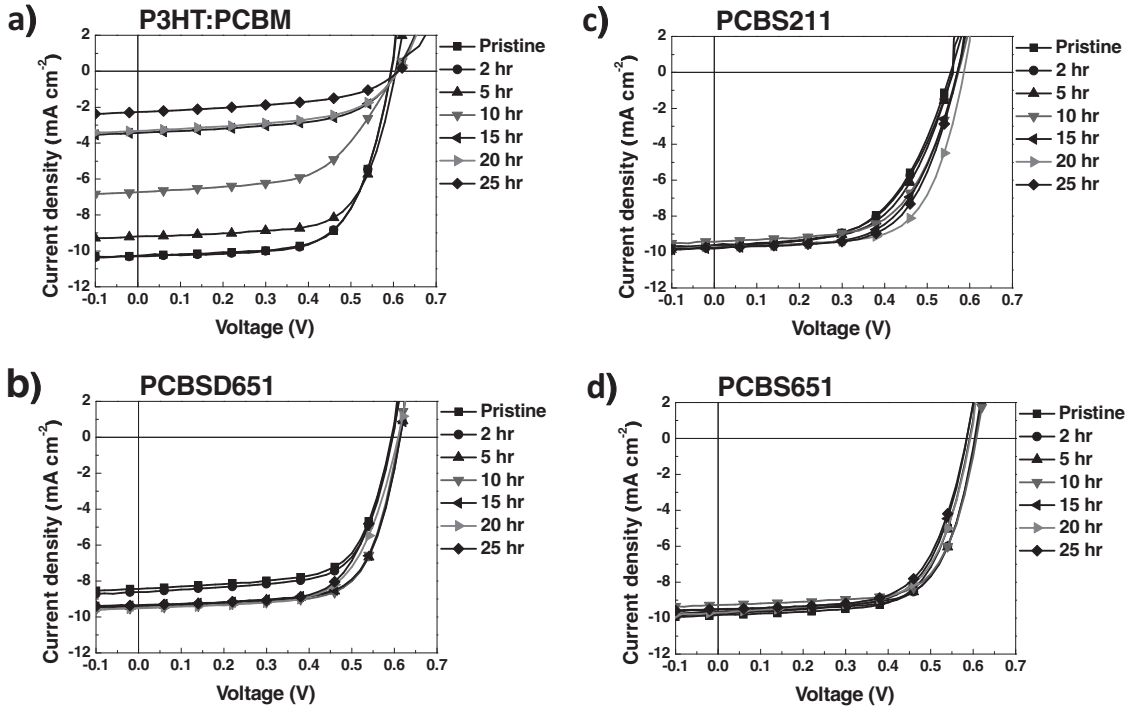

Figure 3. *J–V* characteristics of PSCs based on a) P3HT:PCBM, b) PCBSD561, c) PCBSD211, and d) PCBS651 blends before and after isothermal heating at 150 °C for various times.

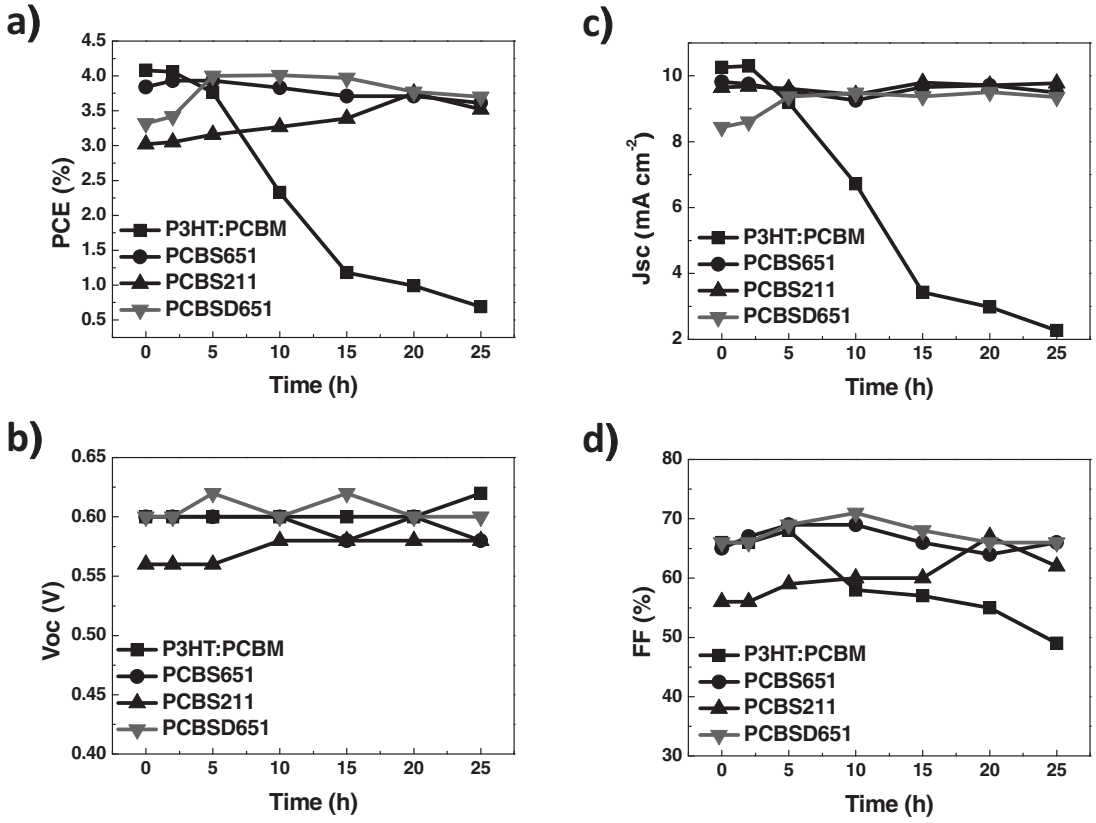

Figure 4. Photovoltaic parameters of PSCs based on the P3HT:PCBM, PCBSD651, PCBS211, and PCBS651 blends as functions of heating time at 150 °C. a) PCE, b) open-circuit voltage (V_{oc}), c) short-circuit current (J_{sc}), and d) fill factor (FF).

time increases. The PCE of the device dropped dramatically from 4.08% to 0.69% after 25 h isothermal heating (Figure 4a). As shown in Figure 4c, the decrease in efficiency is mainly a result of the decrease in J_{sc} values. In sharp contrast, the PCBSD651 device exhibited very stable device characteristics and did not show any degradation after 25 h heating (Figure 3b). We associate the improved stability with several factors. The crosslinked PCBSD, with its highly amorphous nature, will reduce the crystallinity of the fullerene materials.[18] Furthermore, the interconnected PCBSD network in the blend will sterically restrict the mobile PCBM from fast immigration upon thermal heating. Therefore, the large-scale phase separation in the active layer due to PCBM aggregation can be greatly suppressed. Surprisingly, the PCE of PCBSD651 was even increased upon thermal heating, and reached its highest value—4.01%—after 10 h heating. This value is already comparable to the initial performance of the P3HT:PCBM reference device. The thermal-annealing conditions to obtain optimal morphology for the binary P3HT:PCBM and the ternary P3HT:PCBM:PCBSD blends should be very different. Incorporation of the crosslinked PCBSD network into the P3HT:PCBM blend will lead to an altered morphology that is not optimized at the beginning (110 °C for 10 min and 150 °C for 10 min). The continuous thermal annealing of this ternary blend will gradually induce the optimized morphology that results in the improved performance. In view of the fact that only 8% weight content of the PCBSD material in the ternary blend already sufficiently preserves the morphology, the electron-transporter content may be further increased by removing the dendritic moiety in the PCBSD. PCBS, which consists of a simple 4-vinylbenzyl group, was designed to improve the active-C_{60} electron-transporter content relative to PCBSD (71 wt% versus 58 wt%). Again, under the same processing conditions, we fabricated three devices—PCBS101, PCBS211, and PCBS651—based on the three corresponding blend systems—P3HT:PCBM:PCBS (1:0:1 in wt%), P3HT:PCBM:PCBS (2:1:1 in wt%), and P3HT:PCBM:PCBS (6:5:1 in wt%). The *J–V* characteristics of these devices are shown in Figure 2b. Device PCBS101 showed an initial PCE of ca. 2%, which already outperforms the dendron-containing analogue PCBSD101, and even device PCBSD211. Notably, a complete reduction of the kink effects in the *J–V* curves of devices PCBS101 and PCBS211 suggests that increasing the active-C_{60} content indeed greatly improves electron-transport properties. By further decreasing the PCBS content of the blends, devices PCBS211 and PCBS651 achieved the enhanced PCEs of 3.02% and 3.84%, respectively. In a similar manner, the thermal stability of the PCBS211 and PCBS651 devices upon isothermal heating at 150 °C were also evaluated. Encouragingly, both PCBS211 and PCBS651 devices also exhibited very stable device performances against thermal treatment (Figure 3c–d and Figure 4). Considering that the content of active C_{60} in PCBS (71 wt%) is very close to that of PCBM (79 wt%), and the structure of PCBS is very similar to that of PCBM, the active layers containing PCBS as dopant can easily achieve optimal morphology with better electron-transport properties, which leads to improved device

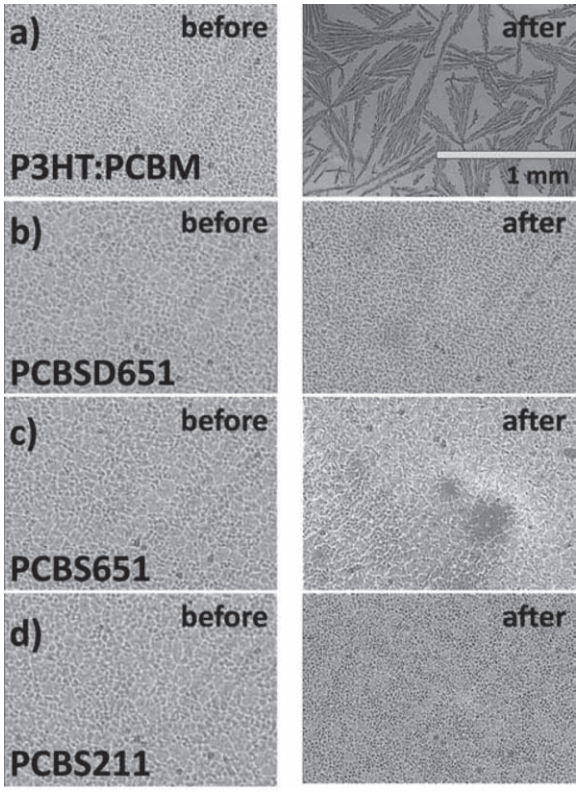

Figure 5. OM images of the blends before and after isothermal heating at 150 °C for 25 h. a) P3HT:PCBM blend, b) PCBSD651 blend, c) PCBS651 blend, and d) PCBS211 blend.

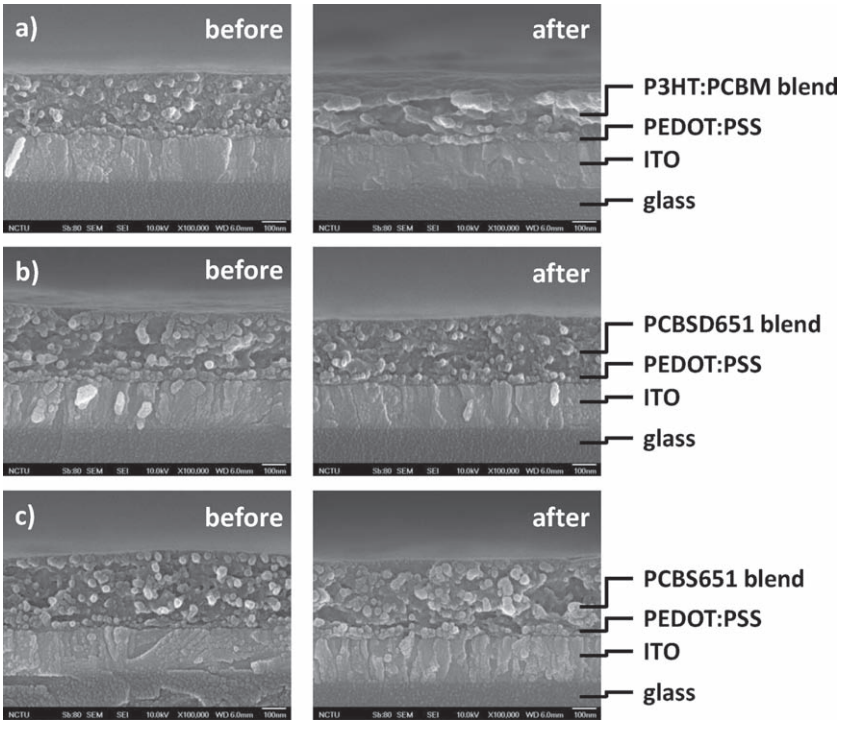

Figure 6. SEM cross-sectional images of the glass/ITO/PEDOT:PSS blends before and after isothermal heating at 150 °C for 25 h. a) P3HT:PCBM blend, b) PCBSD651 blend, and c) PCBS651 blend. The thickness of the photoactive layers is approximately 250 nm.

performance. Most significantly, the low concentration of the polymerized PCBS in the PCBS651 blend (8 wt%) can already fix the optimal morphology to preserve device stability against long-term heating.

2.3. Optical Microscopy (OM) and Scanning Electron Microscopy (SEM)

OM was used to investigate morphological alteration of the blends under the influence of heating (**Figure 5**). Thermal annealing of the P3HT:PCBM blend at 150 °C for 25 h induced a severe macromorphological alteration, giving rise to needle-shaped PCBM crystals of hundreds micrometers in length.[9a,9b,14a] In contrast, the morphology of the PCBSD651 blend remains almost unchanged before and after thermal annealing, which demonstrates the excellent ability of PCBSD to chemically fix the morphology by 3D crosslinking. The polymerizable PCBS, however, shows less ability to effectively lock the morphology. It seems reasonable that the OM images of PCBS651 show some slight local macrographic alteration. In the PCBS211 blend, on the other hand, alteration was completely suppressed due to the higher content of PCBS.

To gain more insight into the microstructure of the active layers on the nanoscale, we also measured the SEM cross-sectional images of the three blends before and after thermal heating (**Figure 6**). The SEM image of the P3HT:PCBM blend showed severe phase segregation after isothermal heating at 150 °C for 25 h. In contrast, the PCBSD651 and PCBS651 blends maintained well-defined nanomorphologies, which again demonstrates that polymerization in the blends is capable of freezing the initially formed morphologies.

2.4. Crystallinity of P3HT in the Blends

The crystallinity of P3HT in the active layer plays an important role in the hole-transport properties. X-ray diffraction (XRD) was employed to detect P3HT crystallinity variations in the blends containing different amounts of PCBSD and PCBS (**Figure 7**).

After thermal annealing at 110 °C for 10 min and 150 °C for 10 min, all of the blends exhibited a sharp 2θ peak centered at ca 5.2° which is the typical signature of well-organized planar P3HT stacks (100) oriented along the axis perpendicular to the substrate.[2a] This means that incorporation of polymerizable n-type materials does not appreciably affect the P3HT crystallinity in the blend. In addition, the first stage of thermal treatment at 110 °C is sufficient for the formation of P3HT crystallites prior to triggering the polymerization at an elevated temperature of 150 °C. Furthermore, the length scales of the P3HT crystallites at the (100) reflection in these blends can be quantified by estimating

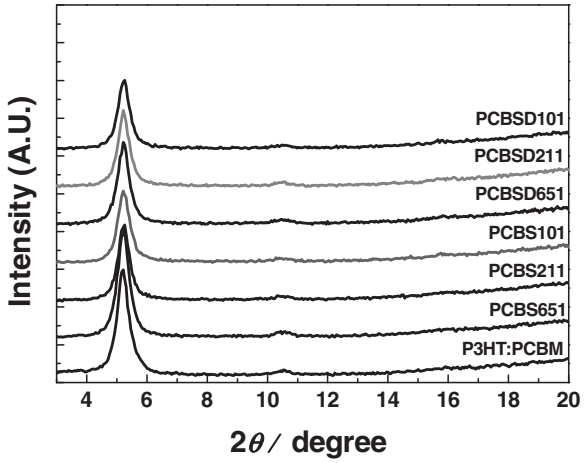

Figure 7. XRD patterns of the P3HT:PCBM, PCBS651, PCBS211, PCBS101, PCBSD561, PCBSD211, and PCBSD101 blends.

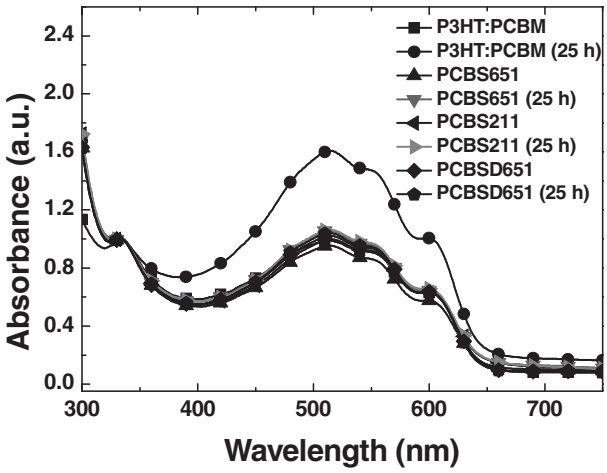

Figure 8. Absorption spectra of the films of the blends before and after 25 h isothermal heating at 150 °C. (a.u. = arbitrary units)

the mean size of the P3HT crystalline domain (τ_{100}) using Scherrer's equation,[19]

$$\tau_{100} \approx \frac{K\lambda}{\beta_{100}\cos\theta} \quad (1)$$

$$\beta_{100} = \Delta_{2\theta} \times \pi/180^{\circ} \quad (2)$$

where K is the shape factor (typically 0.9 for the dimensionless shape factor), and β_{100} is the FWHM intensity of the peak. The mean size of the P3HT crystallite in the P3HT:PCBM blend was determined to be 20.4 nm (see **Table 1**). With increasing PCBSD content in the blend, in conjunction with decreasing PCBM content, the P3HT crystallite size decreases gradually to 18.5 nm for PCBSD651, 17.7 nm for PCBSD211, and 16.2 nm for PCBSD101. In comparison with PCBM, the extra dendritic moiety used for crosslinking in PCBSD will sterically hinder the crystalline growth of P3HT by interfering with the packing order of P3HT. In addition, the amorphous nature of PCBSD before and after polymerization will also enhance its miscibility with P3HT, thereby reducing the crystallization of P3HT to some extent. The same trend can be also observed in the case of the PCBS651 (18.9 nm), PCBS211 (17.7 nm), and PCBS101 (17.3 nm) blends. However, it can be seen that the structural impact of PCBS on the crystallinity of P3HT is less than that of PCBSD.

The optical and photoluminescent properties of the PCBM:P3HT, PCBSD651, PCBS651, and PCBS211 blends were studied before and after thermal heating at 150 °C for 25 h. The absorption and emission spectra of the PCBSD651, PCBS651, and PCBS211 blends are essentially unchanged after thermal heating (**Figure 8** and **Figure 9**); they exhibit absorption peaks at 515, 550, and 610 nm due to the extensive π–π stacking along the P3HT backbone (Figure 8).[20] These results suggest that the polymerization between the PCBSD or PCBS molecules in the blends effectively preserves the morphology of the stacking of P3HT and thus maintains the P3HT absorption and emission properties. However, after 25 h heating, the intensity of the P3HT:PCBM blend in the P3HT absorption region is enhanced, which is again indicative of a higher degree of P3HT crystallization.[9e] Moreover, the P3HT emission intensity in

Table 1. 2θ angle, the full width at half maximum (FWHM) of the P3HT (100) peaks, and the mean size of P3HT crystallites in the blend films.

Blend	2θ [°][a]	$\Delta_2\theta$ [°][b]	τ [nm][c]
P3HT:PCBM	5.22	0.39	20.4
PCBSD651	5.22	0.43	18.5
PCBSD211	5.22	0.45	17.7
PCBSD101	5.23	0.49	16.2
PCBS651	5.23	0.42	18.9
PCBS211	5.22	0.45	17.7
PCBS101	5.22	0.46	17.3

[a]2θ is the angle between the incident and scattered X-ray wavevectors; [b]$\Delta_2\theta$ is the FWHM of the (100) peak; [c]τ is the mean size of the P3HT crystallites determined by Sherrer's equation.

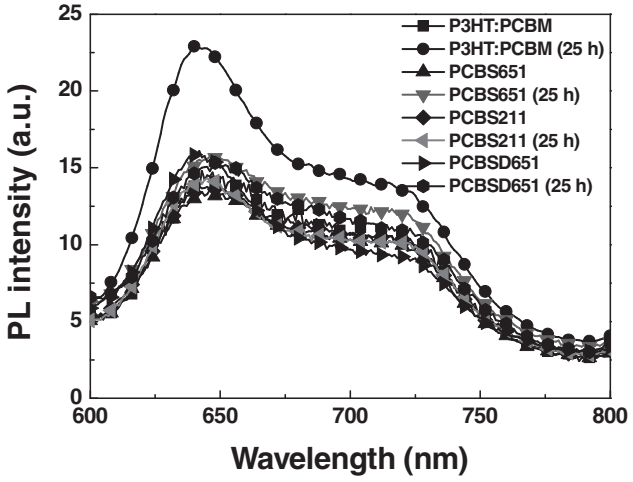

Figure 9. Photoluminescence spectra of the blends before and after isothermal heating at 150 °C for 25 h.

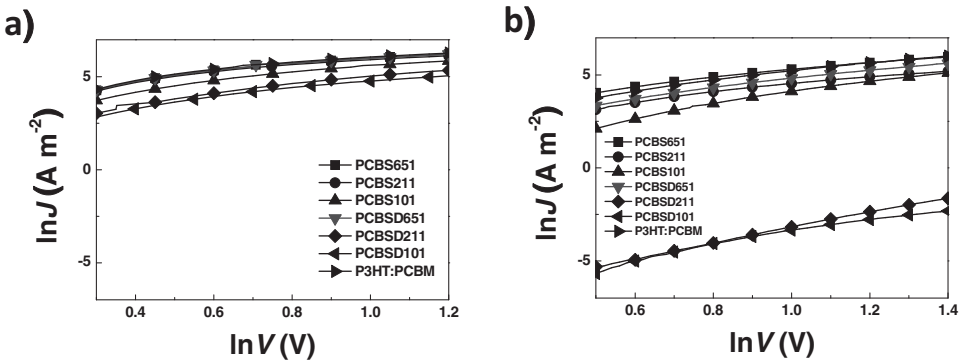

Figure 10. Natural logarithm of *J–V* characteristics of a) the hole-only devices and b) the electron-only devices of PCBS651, PCBS211, PCBS101, PCBSD651, PCBSD211, PCBSD101, and P3HT:PCBM.

the P3HT:PCBM blend is also enhanced 1.6 fold after heating (Figure 9). This implies that the efficiency of exciton dissociation from the P3HT to the PCBM in the blend is reduced.[20b] The prolonged heating destroys the optimal morphology as a result of continuing phase segregation between P3HT and PCBM to a macroscale domain larger than the exciton-diffusion length. The excess P3HT excitons, which cannot reach the D–A interface, will decay through radiative relaxation. The dramatic decrease in the short-circuit current (J_{sc}) (i.e., from 10.26 to 2.27 mA cm^{-2}) of the P3HT:PCBM-based device is therefore strongly associated with the diminution of the interfacial area between the donor and acceptor.

2.5. Carrier Mobilities in the Blends

To quantify the influence of the polymerizable PCBSD and PCBS on the charge-transport characteristics in the active layers, we fabricated a series of unipolar devices to evaluate the hole (**Figure 10**a) and electron (Figure 10b) mobilites of the P3HT:PCBM, PCBSD651, PCBSD211, PCBSD101, PCBS651, PCBS211, and PCBS101 blends by the space–charge limited current (SCLC) technique according to the Mott–Gurney equation:[20a,21]

$$J = \frac{9}{8}\varepsilon\varepsilon_0\mu_0\left(\frac{V^2}{L^3}\right) \quad (3)$$

Table 2. Carrier mobilities of the blends extracted by using the space–charge limited current method.

Blend	Hole mobility, μ_h [cm^{2}s^{-1}V^{-1}]	Electron mobility, μ_e [cm^{2}s^{-1}V^{-1}]	Ratio μ_h/μ_e
P3HT:PCBM	3.10×10^{-4}	1.25×10^{-4}	2.48
PCBS651	2.45×10^{-4}	1.33×10^{-4}	1.84
PCBS211	2.54×10^{-4}	5.96×10^{-5}	4.25
PCBS101	1.76×10^{-4}	4.82×10^{-5}	3.65
PCBSD651	2.98×10^{-4}	8.70×10^{-5}	3.43
PCBSD211	9.54×10^{-5}	8.62×10^{-8}	1107
PCBSD101	7.35×10^{-5}	2.91×10^{-8}	2525

In comparison with the P3HT:PCBM blend, the hole mobility decreases as the content of PCBS or PCBSD increases in the blends. Because the P3HT content is constantly kept at 50 wt% in each blend, variations in the n-type materials do not significantly affect the hole mobility. The slight reduction in hole mobility is also in good agreement with the slightly reduced mean size of the P3HT crystallites in the presence of PCBSD or PCBS. In contrast, the electron mobility decreases dramatically with increasing PCBSD content. The 3D and insulating crosslinking network of PCBSD is an obstacle to the electron transport. On the other hand, PCBS, which contains fewer insulating moieties, exerts much less pronounced effects on the electron transport. The carrier mobilities of the blends are summarized in **Table 2**. It should be noted that the ratio of hole to electron mobility (μ_h/μ_e) increases with PCBSD content. A change of μ_h/μ_e values of more than three orders of magnitude is observed for the PCBSD101 (2525) and PCBSD211 (1107) blends. The less-mobile electrons left behind in the bulk will form a space–charge region thus affecting the *J–V* characteristics of the blend. The low FF values for the PCBSD211 (13%) and PCBSD101 (12%) devices could be attributed to the space–charge buildup caused by the extreme imbalance in carrier mobility. In contrast, the μ_h/μ_e values are all smaller than ten for the other blends; i.e., 1.84 for PCBS651, 4.25 for PCBS211, and 3.43 for PCBSD651. The much more balanced carrier mobility is responsible for the reduction of kink effects in the *J–V* characteristics under AM 1.5.

3. Conclusions

Morphological instability is the primary concern of PSCs. Continuous phase segregation upon heating eventually leads to micron-sized donor–acceptor domains with concomitant reduction of interfacial area. Spherical PCBM with high molecular mobility tends to diffuse out of the polymer matrix and aggregate into larger clusters or single crystals. We have developed a straightforward method to effectively maintain the morphology by in situ polymerization between highly mobile fullerene derivatives to prevent them from severe immigration. Styryl-functionalized polymerizable fullerene derivatives, PCBSD and PCBS, are designed and synthesized for this purpose. Various amounts of PCBSD or PCBS are doped into the P3HT:PCBM

blend to systematically investigate the morphological stability and electron-transport properties. The blending systems were first thermally annealed at 110 °C for 10 min to induce optimal morphology, followed by heating at 150 °C for 10 min to trigger the in situ polymerization of styrene groups. It is found that by doping small amounts of PCBSD into the P3HT:PCBM blend (P3HT:PCBM:PCBSD = 6:5:1 in weight), the initial morphology of the blend can be fixed and preserved effectively after polymerization. The device based on this blend showed highly stable device characteristics, delivering an average PCE of 3.7% during 25 h isothermal heating at 150 °C. In sharp contrast, under the same conditions, the P3HT:PCBM blend undergoes severe phase separation due to the crystallization of P3HT and the aggregation of PCBM. Therefore, the PCE of the P3HT:PCBM-based device dropped dramatically from 4.08% to 0.69%. By removing one styrene group, PCBS, with its higher C_{60} content (71 wt%), possesses better electron-transport properties than PCBSD (58 wt%). Importantly, at a low doping concentration of PCBS in the blend (P3HT:PCBM:PCBS = 6:5:1 in weight), linearly polymerized PCBS can already stabilize the morphology against the heating. This device exhibited more balanced charge mobility to achieve an average PCE of 3.8% during 25 h heating at 150 °C. We envisage that this novel and simple strategy can be widely applied to any other BHJ systems that contain various low-bandgap polymers to achieve highly efficient and morphologically stable polymer solar cells.

4. Experimental Section

Synthesis of PCBS: A 100 ml, two-necked round-bottomed flask was charged with PCBA (26 mg, 0.03 mmol), anhydrous 1,2-dichlorobenzene (20 ml), 4-vinylbenzyl alcohol (3.9 mg, 0.03 mmol), and DMAP (4.25 mg, 0.035 mmol). The solution was cooled to 0 °C with an ice bath, and EDC (5.4 mg, 0.035 mmol) was added in one portion. After stirring at 0 °C for 3 h, the ice bath was removed, and the dark brown reaction mixture was stirred at room temperature for 12 h. After removal of the solvent under reduced pressure, the residue was purified by silica-gel column chromatography with toluene/hexane (1:1 v/v, then pure toluene) as the eluent. The product was redissolved in toluene, and precipitated by adding the solution to methanol. The solid was filtered off and washed with hexane, and then dried under vacuum to yield PCBS as a brown solid (34.6 mg, 69%). ^{1}H NMR (300 MHz, $CDCl_3$, δ): 2.17–2.22 (m, 2 H), 2.5–2.59 (m, 2 H), 2.88–2.93 (m, 2 H), 5.1 (s, 2 H), 5.26 (d, J = 11.4, 1 H), 5.75 (d, J = 17.7, 1 H), 6.66–6.76 (t, 1 H), 7.31–7.41 (m, 4 H), 7.47–7.56 (m, 4 H), 7.91(d, J = 7.5, 1 H); ^{13}C NMR (125 MHz, $CDCl_3$, δ): 22.4, 33.6, 34.1, 51.8, 66.1, 79.8, 114.4, 126.4, 128.2, 128.4, 128.5, 132.1, 135.3, 136.3, 136.7, 137.6, 138.0, 140.7, 140.9, 142.12, 142.17, 142.20, 142.92, 142.98, 143.0 143.1, 143.8, 144.0, 144.4, 144.5, 144.7, 145.03, 145.07, 145.13, 145.18, 145.8, 147.8, 148.8, 172.9.

XRD Measurements: To produce samples with identical film thickness for XRD measurement, blend films were spun on top of the PEDOT:PSS layer. The film thickness of ca 250 nm was confirmed by alpha-step profilometer and cross-sectional SEM. XRD spectra of the samples were obtained using a Bruker D8 Advance spectrophotometer with $Cu_K\alpha$ radiation.

SEM Measurements: Cross-sectional SEM images were measured by using a field-emission SEM equipped with a cold field-emission-type gun (JEOL JSM-7401F, Japan).

Device Fabrication and Measurements: ITO-coated glass substrates (provided by RiTdisplay corp.) were ultrasonicated in deionized (DI) water with 2% detergent, acetone, and isopropyl alcohol for 10 min, respectively, and subsequently dried under a stream of nitrogen. A filtered dispersion of PEDOT:PSS in aqueous solution (Baytron PVP AI-4083) was spuncast at 2000 rpm for 30 s to produce a 30 nm thick layer, followed by baking at 150 °C for 30 min. Seven different solutions of P3HT (20 mg) and fullerene derivatives (totally 20 mg) in 1 g of *o*-DCB were prepared separately with fixed blend-weight ratio of P3HT to the total n-type materials (i.e., PCBM, PCBSD, PCBS) equal to 1:1, and the relative content was adjusted between either PCBM and PCBSD or PCBM and PCBS (as shown in Table 1 in the Supporting Information). The solutions were stirred at 70 °C overnight under a nitrogen atmosphere. Prior to use, the solutions were filtered by passing through a 0.45 μm Teflon syringe filter. For BHJ solar-cell devices and unipolar devices for SCLC measurement, the blend solutions containing polymer/fullerene (1:1, w/w) were spun at 700 rpm for 30 s to form a 250 nm film on top of the PEDOT:PSS layer. Films were dried in covered Petri dishes for 20 min to perform solvent-assisted annealing. The films were then subjected to two-stage thermal annealing, firstly at 110 °C for 10 min and subsequently at 150 °C. Finally, the top electrode, made of Ca (10 nm)/Al (100 nm), was thermally evaporated at a pressure below 10^{-6} torr to complete the BHJ solar-cell devices. To perform the accelerated performance test, BHJ solar-cell devices were subjected to sustained heating at 150 °C for various times prior to the cathode electrode deposition. All the devices were measured at room temperature under a nitrogen atmosphere with a Xenon lamp coupled to an AM 1.5G solar filter (SAN-EI XES-301S solar simulator). *J–V* characteristics were recorded with a Keithley 2400 Source Measurement Unit. The active area was 0.04 cm^2.

Supporting Information

Supporting Information is available from the Wiley Online Library or from the author.

Acknowledgements

This work was supported by the National Science Council and "ATU Plan" of the National Chiao Tung University and Ministry of Education, Taiwan.

Received: November 26, 2010
Published online: March 17, 2011

[1] a) J. J. M. Halls, K. Pichler, R. H. Friend, S. C. Moratti, A. B. Holmes, *Appl. Phys. Lett.* **1996**, *68*, 3120; b) M. Theander, A. Yartsev, D. Zigmantas, V. Sundström, W. Mammo, M. R. Andersson, O. Inganäs, *Phys. Rev. B* **2000**, *61*, 12957; c) A. Haugeneder, M. Neges, C. Kallinger, W. Spirkl, U. Lemmer, J. Feldmann, U. Scherf, E. Harth, A. Gügel, K. Müllen, *Phys. Rev. B* **1999**, *59*, 15346; d) T. Stübinger, W. Brütting, *J. Appl. Phys.* **2001**, *90*, 3632; e) D. E. Markov, E. Amsterdam, P. W. M. Blom, A. B. Sieval, J. C. Hummelen, *J. Phys. Chem. A* **2005**, *109*, 5266; f) Y.-J. Cheng, S.-H. Yang, C.-S. Hsu, *Chem. Rev.* **2009**, *109*, 5868.

[2] a) W. Ma, C. Yang, X. Gong, K. Lee, A. J. Heeger, *Adv. Funct. Mater.* **2005**, *15*, 1617; b) A. C. Mayer, S. R. Scully, B. E. Hardin, M. W. Rowell, M. D. McGehee, *Mater. Today* **2007**, *10*, 28; c) M. Reyes-Reyes, K. Kim, D. L. Carroll, *Appl. Phys. Lett.* **2005**, *87*, 083506; d) C. H. Woo, B. C. Thompson, B. J. Kim, M. F. Toney, J. M. J. Fréchet, *J. Am. Chem. Soc.* **2008**, *130*, 16324.

[3] Y. Kim, S. Cook, S. M. Tuladhar, S. A. Choulis, J. Nelson, J. R. Durrant, D. D. C. Bradley, M. Giles, I. McCulloch, C.-S. Ha, M. Ree, *Nat. Mater.* **2006**, *5*, 197.

[4] M. Koppe, C. J. Brabec, S. Heiml, A. Schausberger, W. Duffy, M. Heeney, I. McCulloch, *Macromolecules* **2009**, *42*, 4661.

[5] R. C. Hiorns, R. de Bettignies, J. Leroy, S. Bailly, M. Firon, C. Sentein, A. Khoukh, H. Rreudhomme, C. Dagron-Lartigau, *Adv. Funct. Mater.* **2006**, *16*, 2263.
[6] a) H. Hoppe, M. Niggenmann, C. Winder, J. Kraut, R. Hiesgen, A. Hinsch, D. Meissner, N. S. Sariciftci, *Adv. Funct. Mater.* **2004**, *14*, 1005; b) D. Chirvase, J. Parisi, J. C. Hummelen, V. Dyakonov, *Nanotechnology* **2004**, *15*, 1317.
[7] a) G. Li, V. Shrotriya, J. Huang, Y. Yao, T. Moriarty, K. Emery, Y. Yang, *Nat. Mater.* **2005**, *4*, 864; b) F. Padinger, R. S. Rittberger, N. S. Sariciftci, *Adv. Funct. Mater.* **2003**, *13*, 85; c) L. H. Nguyen, H. Hoppe, T. Erb, S. Günes, G. Gobsh, N. S. Sariciftci, *Adv. Funct. Mater.* **2007**. *17*, 1071; d) M. Reyes-Reyes, K. Kim, J. Dewald, R. López-Sandoval, A. Avadhanula, S. Curran, D. L. Carroll, *Org. Lett.* **2005**, *7*, 5749; e) H. Hoppe, T. Glatzel, M. Niggemann, A. Hinsch, M. C. Lux-Steiner, N. S. Sariciftci, *Nano Lett.*, **2005**, *5*, 269; f) G. Li, Y. Yao, H. Yang, V. Shrotriya, G. Yang, Y. Yang, *Adv. Funct. Mater.* **2007**, *17*, 1636; g) A. L. Ayzner, D. D. Wanger, C. J. Tasson, S. H. Tolbert, B. J. Schwartz, *J. Phys. Chem. C* **2008**, *112*, 18711; h) L. H. Nguyen, H. Hoppe, T. Erb, S. Günes, G. Gobsch, N. S. Sariciftci, *Adv. Funct. Mater.* **2007**, *17*, 1071.
[8] H. Hoppe, N. S. Sariciftci, *J. Mater. Chem.* **2006**, *16*, 45 and references therein.
[9] a) E. Klimov, W. Li, X. Yang, G. G. Hoffmann, J. Loos, *Macromolecules* **2006**, *39*, 4493; b) Y.-C. Huang, S.-Y. Chuang, M.-C. Wu, H.-L. Chen, C.-W. Chen, W.-F. Su, *J. Appl. Phys.* **2009**, *106*, 034506; c) H. Zhong, X. Yang, B. deWith, J. Loos, *Macromolecules* **2006**, *39*, 218; d) X. Yang, J. K. J. van Duren, R. A. J. Janssen, M. A. J. Michels, J. Loos, *Macromolecules* **2004**, *37*, 2151; e) A. Swinnen, I. Haeldermans, M. vande Ven, J. D'Haen, G. Vanhoyland, S. Aresu, M. D'Olieslaeger, J. Manca, *Adv. Funct. Mater.* **2006**, *16*, 760; f) C. Muller, T. A. M. Ferenczi, M. Campoy-Quiles, J. M. Frost, D. D. C. Bradley, P. Smith, N. Stingelin-Stutzmann, J. Nelson, *Adv. Mater.* **2008**, *20*, 3510.
[10] X. Yang, J. K. J. van Duren, M. T. Rispens, J. C. Hummelen, R. A. J. Janssen, M. A. J. Michels, J. Loos, *Adv. Mater.* **2004**, *16*, 802.
[11] M. Jørgensen, K. Norrman, F. C. Krebs, *Sol. Energy Mater. Sol.Cells* **2008**, *92*, 686.
[12] K. Sivula, C. K. Luscombe, B. C. Thompson, J. M. J Fréchet, *J. Am. Chem. Soc.* **2006**, *128*, 13988.
[13] a) K. Sivula, Z. T. Ball, N. Watanabe, J. M. J. Fréchet, *Adv. Mater.* **2006**, *18*, 206; b) Z. Zhou, X. Chen, S. Holdcroft, *J. Am. Chem. Soc.* **2008**, *130*, 11711; c) J. B. Kim, K. Allen, S. J. Oh, S. Lee, M. F. Toney, Y. S. Kim, C. R. Kagan, C. Nuckolls, Y.-L. Loo, *Chem. Mater.* **2010**, *22*, 5762; d) N. Camaioni, M. Catellani, S. Luzzati and A. Migliori, *Thin Solid Films*, **2002**, *403*, 489.
[14] a) B. J. Kim, Y. Miyamoto, B. Ma, J. M. J. Fréchet, *Adv. Funct. Mater.* **2009**, *19*, 2273; b) B. Gholamkhass, S. Holdcroft, *Chem. Mater.* **2010**, *22*, 5371; c) Z. Zhu, S. Hadjikyriacou, D. Wallker, R. Gaudiana, *J. Macromol. Sci., Part A: Pure Appl. Chem.* **2004**, *41*, 1467; d) M. Drees, H. Hoppe, C. Winder, H. Neugebauer, N. S. Sariciftci, W. Schwinger, F. Schäffler, C. Topf, M. C. Scharber, Z. Zhu, R. Gaudiana, *J. Mater. Chem.* **2005**, *15*, 5158; e) J.-F. Nierengarten, S. Setayesh, *New J. Chem.* **2006**, *30*, 313.
[15] E. Zhou, Z. Tan, C. Yang, Y. Li, *Macromol. Rapid Commun.* **2006**, *27*, 793.
[16] a) Y.-J. Cheng, M. S. Liu, Y. Zhang, Y. Niu, F. Huang, J.-W. Ka, H.-L. Yip, Y. Tian, A. K.-Y. Jen, *Chem. Mater.* **2008**, *20*, 413; b) F. Huang, Y.-J. Cheng, Y. Zhang, M. S. Liu, A. K.-Y. Jen, *J. Mater. Chem.* **2008**, *18*, 4495.
[17] C.-H. Hsieh, Y.-J. Cheng, P.-J. Li, C.-H. Chen, M. Dubosc, R.-M. Liang, and C.-S. Hsu, *J. Am. Chem. Soc.* **2010**, *132*, 4887.
[18] Y. Zhang, H.-L. Yip, O. Acton, S. K. Hau, F. Huang, A. K.-Y. Jen, *Chem. Mater.* **2009**, *21*, 2598.
[19] a) M.-Y. Chiu, U-S. Jeng, C.-H. Su, K. S. Liang, K.-H. Wei, *Adv. Mater.* **2008**, *20*, 2573; b) T. Erb, U. Zhokhavets, G. Gobsch, S. Raleva, B. Stühn, P. Schilinsky, C. Waldauf, C. J. Brabec, *Adv. Funct. Mater.* **2005**, *15*, 1193.
[20] a) G. Zhao, Y. He, Z. Xu, J. Hou, M. Zhang, J. Min, H.-Y. Chen, M. Ye, Z. Hong, Y. Yang, Y. Li, *Adv. Funct. Mater.* **2010**, *20*, 1480; b) L.-M. Chen, Z. Hong, W. L. Kwan, C.-H. Lu, Y.-F. Lai, B. Lei, C.-P. Liu, Y. Yang, *ACS nano* **2010**, *4*, 4744.
[21] C. Goh, R. J. Kline, M. D. McGehee, E. N. Kadnikova, J. M. J. Fréchet, *Appl. Phys. Lett.* **2005**, *86*, 122110.